Controlled oxidation of FeCo magnetic nanoparticles to produce faceted FeCo/ferrite nanocomposites for rf heating applications

K. N. Collier,[1,2] N. J. Jones,[1] K. J. Miller,[1] Y. L. Qin,[1] D. E. Laughlin,[1] and M. E. McHenry[1,2]

[1]*Department of Materials Science and Engineering, Carnegie Mellon University, Pittsburgh, Pennsylvania 15213, USA*

[2]*Department of Biomedical Engineering, Carnegie Mellon University, Pittsburgh, Pennsylvania 15213, USA*

We report the oxidation products and qualitative rates for polydisperse FeCo magnetic nanoparticles (MNPs) synthesized using an induction plasma torch. X-ray diffraction (XRD) and TEM showed MNPs to have a thin ferrite shell. Nanopowders were isochronally annealed to promote oxidation and XRD was used to follow the evolution of the FeCo core and the Fe_3O_4 and FeO oxide shells. Isothermal anneals were used to follow oxidation kinetics at 350 and 500 °C. High resolution transmission electron microscopy (HRTEM) revealed faceted morphologies terminated at (100) and (110) FeCo faces with $(110)_{FeCo} \| (111)_{oxide}$ and $(100)_{FeCo} \| (100)_{oxide}$, and $[010]_{FeCo} \| [011]_{oxide}$ orientation relationships between the FeCo core and oxide shell. We show HRTEM images of MNP chaining and compare the rf heating of samples of aqueous ferrofluids similarly loaded with as synthesized and oxidized MNPs. © *2009 American Institute of Physics*. [DOI: 10.1063/1.3054376]

INTRODUCTION

We report a systematic study of the oxidation products and rates for plasma torch synthesized FeCo nanoparticles.[1] FeCo nanoparticles are being studied in applications including radio-frequency (rf) heating for thermoablative cancer therapies[2] and magnetomechanical response in tissue scaffolds.[3] This work furthers the understanding of nanostructural evolution and oxidation products in FeCo/ferrite nanocomposite materials and their influence on applications.[4]

We report the sequence of oxide formation and epitaxial relationships with polyhedral facetted magnetic FeCo nanoparticles and the role of Néel relaxation in the rf field activated heating of two-phase FeCo/ferrite MNPs.

FeCo nanoparticles are unique in forming stable ferrite coatings for which the oxidation kinetics are sluggish at room temperature (RT). If adherent biocompatible oxide shells are engineered and functionalized with surfactants to stabilize aqueous ferrofluids, MNPs can bind to antibodies to promote cell or tissue attachment and efficient point source heating of nanoparticles can be exploited for thermoablative cancer therapies. The oxide coatings provide polar surfaces for attachment of surfactants and protect the high magnetic moment FeCo core from corrosion. FeCo/ferrite nanocomposites have FeCo cores with (100) and (110) face truncations, in contrast to previously observed (100) and (111) facets in spinel ferrite MNPs.[5] This offers the possibility of exploring oxidation rates through specific facets, preferential surface attachment of surfactants, and the role of surface crystallography on exchange bias between oxide shells and FeCo cores.

EXPERIMENTAL PROCEDURE

Polydisperse $Fe_{50}Co_{50}$ MNPs were synthesized using a 50 kW, 3 MHz rf Tekna induction plasma torch (PT).[3] We started with $Fe_{50}Co_{50}$ alloy precursor powders produced by gas atomization[6] and sieved to <53 μm. Consistent with

previous experience,[7] the resulting PT FeCo MNPs had a thin adherent (Fe,Co)-ferrite shell. Initial Mössbauer spectroscopy studies indicate that the oxide has Co-rich and Fe-rich layers.[8]

Structural characterization was carried out by conventional x-ray diffraction (XRD) on powders using a Rigaku powder diffractometer. In order to reveal their crystal structure, a step size of 0.1 seconds was used, a voltage of 35 keV, a range of 25–105° 2θ using a Cu tube with $K\alpha$ radiation. A Scherrer analysis was performed on these powders and indicated an average particle size of 35 nm (by volume weighting).

A more direct tool for determining particle size is the transmission electron microscope (TEM). Particle size distributions for the PT synthesized nanoparticles were determined using a JEOL 2000EX TEM. The sizes of the particles were fit to a log-normal distribution with a geometric mean of 19.7 nm and a standard deviation of 8.5 nm. These measurements reinforce observations[9] that different techniques yield different values depending on the weighting scheme. High resolution transmission electron microscopy (HRTEM) was performed on a Tecnai F20 TEM to create a three-dimensional (3D) morphology of the nanoparticles.

Isochronal oxidation studies were performed between 100 and 1000 °C for 2 h. The powder samples were then characterized by conventional XRD. Isothermal kinetics of oxidation were studied at 350 and 500 °C. 1–2 g samples of the as-PT synthesized powders were heated for 15, 30, 60, 180, 360, and 1440 min. XRD results of the kinetics of oxidation are not discussed here.

dc magnetic properties were studied using a Lakeshore vibrating sample magnetometer (VSM) equipped with a furnace that can operate to 1300 K. Heating of the MNPs in ferrofluids was performed using an AMERITHERM Hotshot rf power supply. This has a 280 kHz maximum power supply operated at 100 A through a three-turn coil. Heating rates of
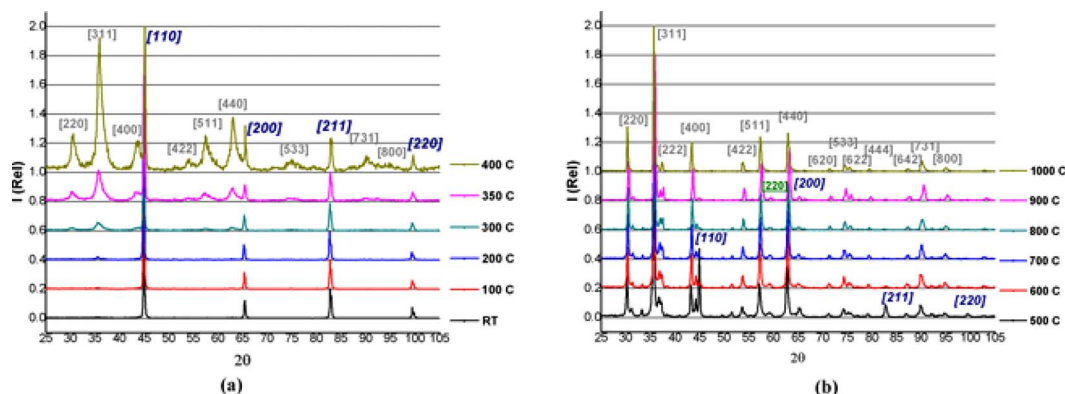
FIG. 1. (Color online) XRD patterns of FeCo nanoparticles showing oxidation between (a) RT and 400 °C and (b) 500 and 1000 °C for 2 h. Dark labels show FeCo peaks, light labels show Fe_3O_4 peaks, and the underlined [220] label shows an FeO peak.

aqueous ferrofluids with as-PT synthesized FeCo and FeCo oxidized for 2 h at 350 and 600 °C were observed. Ferrofluids of 10 wt % FeCo functionalized in 2 mM polyethylene oxide (PEO) surfactant solution were heated in the rf coil at 100 A from room temperature. Ferrofluids containing equivalent magnetization of FeCo were also heated by this process. Concentrations of equivalent magnetization ferrofluids were 9.1 wt % of as-PT synthesized powder, 10 wt % of powder oxidized for 2 h at 350 °C, and 18.3 wt % of powder oxidized for 2 h at 600 °C. A Luxtron optical fiber thermometer was used for temperature measurement with data collected every 2 s.

RESULTS AND DISCUSSION

The measured XRD patterns for varying temperatures are shown in Figs. 1(a) and 1(b), respectively. XRD analysis shows FeCo peaks at low temperatures with nominal ferrite peaks. Oxidation occurs gradually until 300 °C and more rapid oxidation occurs at 350 °C and above, showing peaks for the spinel ferrite $(Fe,Co)_3O_4$. At temperatures greater than 900 °C, FeO peaks are observed and FeCo peaks are no longer present.

In Fig. 1, it can be seen that magnetite (Fe_3O_4) is the first oxide to appear with no hematite peaks discernible in the high temperature oxidation experiments; wustite (FeO) is observed at the higher oxidation temperatures tested. This pro-

gression of oxidation agrees with the sequence for iron as proposed by Birks *et al.*[10] Wustite will only form at temperatures above 570 °C, which confirms its absence at lower temperatures. At lower temperatures, magnetite will form first and will comprise a large fraction of the oxide layer with hematite forming only a thin layer at the interface between the oxide and the air atmosphere. During initial oxidation, the oxygen partial pressure will be high as will the presence of Fe/Co at the surface. This will favor a 1:1 ratio of Fe/Co to O in the oxide. Due to the instability of wustite, Fe_3O_4 will form. This will occur until the layer is large enough that the Fe/Co mobility is low and much of the Fe/Co at the surface is tied up in magnetite. At this point, hematite will form.

At higher temperatures, wustite should be seen in greater amounts due to its high defect mobility. This is not seen, however, in the XRD data, except for a few small peaks. This may be due to the technique of oxidation and furnace temperature lag time. After the formation of magnetite, wustite can form; however it will depend on the mobility of large oxygen anions through the magnetite layer in order to react with the Fe/Co surface. Since it is difficult to discern Fe from Co in the XRD data, a more in depth study of the oxide layer will be the subject of future work using Mössbauer, Auger, and x-ray photoelectron spectroscopies to understand
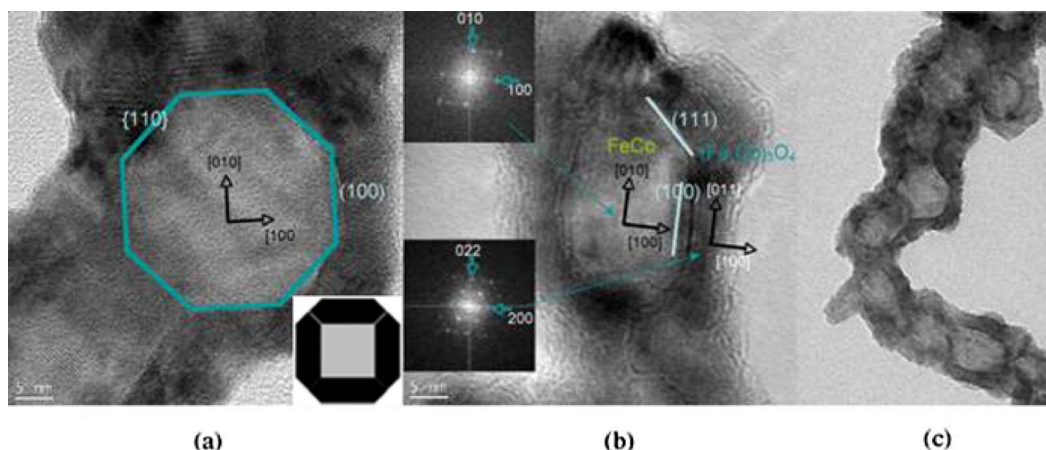

FIG. 2. (Color online) (a) An FeCo particle (oxidized 24 h at 350 °C) with an octagonal like projection [inset: simulated representation of a (110)-truncated cube using KRYSTALSHAPER™ software]. (b) An HRTEM of an FeCo particle (oxidized 6 h at 350 °C) showing ORs between it and its oxide and (c) low resolution image of the chaining of particles (oxidized 24 h at 350 °C).
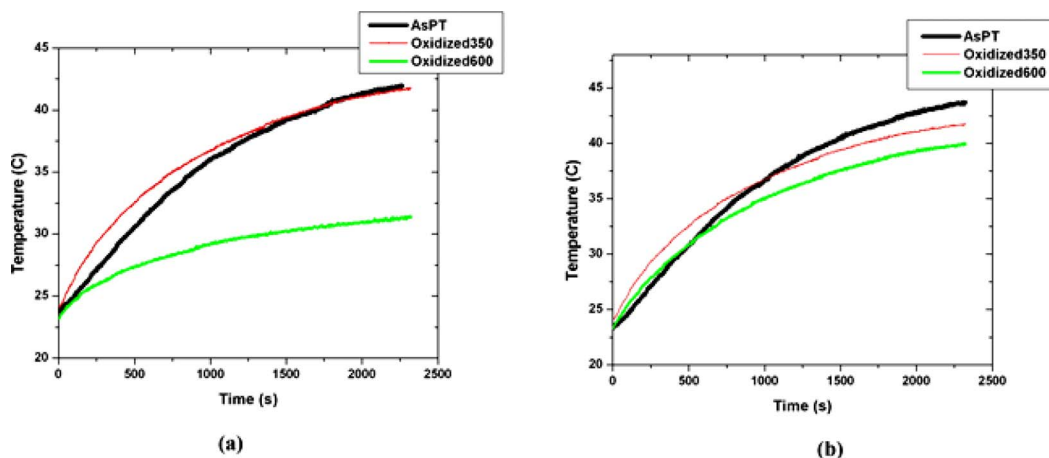
FIG. 3. (Color online) (a) Heating rates of 10 wt % FeCo in PEO ferrofluids with powders of varying states of oxidation. While as-PT powders and those oxidized at 350 °C powders show similar heating rates, powders oxidized at 600 °C heat significantly slower. (b) Heating curves for ferrofluids with equal magnetization.

the nature of the oxide layer.

The oxidation kinetics were then followed more closely at 350 and 500 °C for various lengths of time. At 350 °C significant oxidation occurred after only 15 min and remained gradual until oxidation increased more rapidly at times longer than 6 h. Oxidation occurred more rapidly at 500 °C and was nearly fully oxidized after 1.5 h.

A TEM determined nanoparticle log-normal size distribution indicated $\mu = 19.7$ nm and $\sigma = 8.5$ nm. HRTEM showed MNPs to have a thin adherent ferrite shell. The FeCo particle in Fig. 2(a) is seen to have an octagonal-like projection. Such a projected image, from a cubic crystal, could come from a (111)-truncated cube having 14 faces consisting of {100} and {111} facets or from a (110)-truncated cube having 18 faces consisting of facets of the type {110} and {100}. Since the FeCo particle is either bcc or a derivative ordered structure of bcc (B2) it is likely that the particle has {110} facets and not {111} facets as the {110} planes are low energy in a bcc structure. A schematic of the projection of such an 18 sided particle is shown in the inset of Fig. 2(a).

The FeCo particle shown in Fig. 2(b) reveals one full orientation relationship (OR) between the FeCo particle and its oxide. From the fast Fourier transforms of the high resolution images the ORs can be seen to be

$$(100)_{\text{FeCo}} \parallel (100)_{\text{oxide}} \quad \text{and} \quad [010]_{\text{FeCo}} \parallel [011]_{\text{oxide}}.$$

The oxide forms first on the {100} facets of the FeCo particle because of a close lattice match between {100} of FeCo and {100} of the oxide with $\langle 110 \rangle$oxide$\parallel \langle 100 \rangle$FeCo. These oxide regions then grow around the particle and meet at {110} facets of the FeCo at a twinlike boundary between them.

The heating rate data of the 10 wt % ferrofluids in Fig. 3(a) show little difference between the as-PT powder and the 350 °C oxidized powder, but a significant decrease in heating of the powder oxidized at 600 °C. VSM data of the powders show relatively close saturation magnetization values for as-PT and 350 °C oxidized powders while the M_s of the 600 °C oxidized powder is nearly half that of the as-PT, which explains the low heating rate due to low magnetization in $(\text{Fe},\text{Co})_3\text{O}_4$ compared to FeCo. Peak heating rates are expected at particle sizes smaller than the average diameter

of the as-PT FeCo powder.[11] The particles' oxide grows at the expense of the FeCo, decreasing the size of the core; however the heating rates of the equivalent magnetization ferrofluids were observed to decrease slightly with more oxidation and smaller FeCo core sizes. The apparent effect is small because PT synthesized MNPs are very polydisperse and oxidation has only a small measurable effect on the average particle diameter. Another factor that may contribute to the difference of heating rates is the change in the anisotropy constant of the overall material as the thickness of the oxide increases and FeCo decreases.

ACKNOWLEDGMENTS

[1] Z. Turgut, M.-Q. Huang, K. Gallagher, S. A. Majetich, and M. E. McHenry, J. Appl. Phys. **81**, 4039 (1997); Z. Turgut, J. H. Scott, S. A. Majetich, and M. E. McHenry, *ibid.* **83**, 6468 (1998).
[2] A. H. Habib, C. L. Ondeck, P. Chaudhary, M. R. Bockstaller, and M. E. McHenry, J. Appl. Phys. **103**, 07A307 (2008).
[3] T. W. Gilbert, A. M. Stewart-Akers, and S. F. Badylak, Biomaterials **28**, 147 (2007).
[4] K. J. Miller, K. N. Collier, H. B. Soll-Morris, R. Swaminathan, and M. E. McHenry, J. Appl. Phys.(this conference).
[5] R. Swaminathan, M. E. McHenry, P. Poddar, and H. Srikanth, J. Appl. Phys. **97**, 10G104 (2005).
[6] Gas atomized powders were provided by Z. Turgut, AFRL-WPAFB.
[7] Z. Turgut, N. T. Nuhfer, H. R. Piehler, and M. E. McHenry, J. Appl. Phys. **85**, 4406 (1999).
[8] M. Sorescu, personal communication (1/24/2008).
[9] M. A. Willard, L. K. Kurihara, E. E. Carpenter, S. Calvin, and V. G. Harris, Int. Mater. Rev. **49**, 125 (2004).
[10] N. Birks, G. H. Meier, and F. S. Pettit, *Introduction to the High-Temperature Oxidation of Metals*, 2nd ed. (Cambridge University Press, New York, 2006).
[11] R. E. Rosensweig, J. Magn. Magn. Mater. **252**, 370 (2002).